Structure and ferroelectric properties of $[C_3N_2H_5]_5[Bi_2Br_{11}]$

2008 J. Phys.: Condens. Matter 20 325224

(http://iopscience.iop.org/0953-8984/20/32/325224)

J. Phys.: Condens. Matter **20** (2008) 325224 (9pp) doi:10.1088/0953-8984/20/32/325224

Structure and ferroelectric properties of $[C_3N_2H_5]_5[Bi_2Br_{11}]$

A Piecha, A Białońska and R Jakubas

Faculty of Chemistry, University of Wrocław, Joliot-Curie 14, 50-383 Wrocław, Poland

E-mail: rj@wchuwr.chem.uni.wroc.pl

Received 25 April 2008, in final form 21 June 2008
Published 18 July 2008
Online at stacks.iop.org/JPhysCM/20/325224

Abstract

A ferroelectric crystal $[C_3N_2H_5]_5[Bi_2Br_{11}]$ has been synthesized and structurally characterized at 170 and 100 K. The crystal structure consists of discrete corner-sharing bioctahedra $[Bi_2Br_{11}]^{5-}$ and highly disordered imidazolium cations. The room temperature crystal structure has been determined as monoclinic, space group, $P2_1/n$ with: $a = 9.257(2)$ Å, $b = 15.157(3)$ Å, $c = 13.865(3)$ Å and $\beta = 97.73(3)°$. The crystal undergoes two solid–solid phase transitions: at 355 K of first-order and at 155 K of second-order type. The later transition takes place between monoclinic phases: $P2_1/n \rightarrow Pn$. The dielectric and pyroelectric measurements allow us to characterize the low temperature phase III as ferroelectric with the Curie temperature at 155 K. The saturated spontaneous polarization of the order of 2.6×10^{-3} C m^{-2} was measured along the a-axis (130 K). The ferroelectric phase transition mechanism at 155 K is due to the dynamics of three of five nonequivalent imidazolium cations.

(Some figures in this article are in colour only in the electronic version)

1. Introduction

Hybrid organic–inorganic crystals evoke much interest because they frequently exhibit ferroelectric and magnetic ordering. From an application point of view special attention has been paid to their nonlinear-optical properties, electroluminescence and photoluminescence [1–4]. Among them, halogenoantimonates (III) and halogenobismuthates (III) of the general formula $R_aM_bX_{(3b+a)}$ (where R denotes the organic cation, M denotes the metal Sb(III) or Bi(III) and X denotes a halogen atom: Cl, Br, I) have been found to possess interesting ferroic/ferroelectric properties. Ferroelectricity is characteristic of compounds which crystallize with chemical compositions; $R_3M_2X_9$ and $R_5M_2X_{11}$. An anionic substructure plays a key-role in the generation of ferroelectric properties [5–10]. Five possible anionic substructures in crystalline lattice of the $R_3M_2X_9$ subgroup are known: one-dimensional chains, two-dimensional layers, discrete bioctahedra, discrete tetramers and two-dimensional units. In this subgroup, the compounds with two-dimensional anionic substructure reveal a tendency to exhibit ferroelectricity [11, 12]. In turn, all known compounds of $R_5M_2X_{11}$ type contain discrete bioctahedra (two octahedra connected one to each other by only one halogen atom) in the crystalline lattice. To the best of our knowledge, five compounds crystallizing with this composition are known [13–17], and all of them reveal ferroelectricity. The ferroelectricity of either $R_3M_2X_9$ or $R_5M_2X_{11}$ subgroups has been explained in terms of the motion of strongly dipolar organic cations (methylammonium [18], pyridinium [15] and imidazolium [19, 20]). In particular, the compounds of $R_5M_2X_{11}$ type have been the subject of considerable investigations over a dozen years. The interest has arisen primarily from the fact that the methylammonium analogs being ferroelectric at room temperature [21, 22], possess the dielectric characteristics, which are comparable to those found in the well-known TGS-family (triglycine sulfate) of crystals [23]. Replacement of small methylammonium cations by larger size pyridinium or imidazolium ones, shifts the ferroelectric phase towards lower temperature, thus polar properties were found to appear below 160–150 K [16, 17]. Although numerous papers have been devoted to studies of the physical properties of $R_5M_2X_{11}$-type compounds the origin of ferroelectricity in these salts is still unclear. In this paper, we present the results of single crystal x-ray measurements (at 170 and 100 K), calorimetric, dielectric and pyroelectric studies on a novel ferroelectric compound pentakis (imidazolium) undecabromodibismuthate (III); $[C_3N_2H_5]_5[Bi_2Br_{11}]$. The mechanism of the paraelectric–ferroelectric phase transition taking place in this compound at 155 K is briefly discussed.

2. Experiments

The starting materials were commercial $BiBr_3$ (99.999%, Aldrich), imidazole amine—$C_3N_2H_4$ (99.5%, Fluka) and HBr (48%, Sigma-Aldrich). A sample of $[C_3N_2H_5]_5[Bi_2Br_{11}]$ was prepared by the reaction of stoichiometric amounts of $BiBr_3$ and imidazole (molar ratio 3:1) in concentrated HBr at about 360 K. The desired product was twice recrystallized from water. Yellow and transparent single crystals were grown by a slow evaporation from an aqueous solution that contained some amounts of hydrobromic acid to prevent the hydrolysis of $BiBr_3$ at constant room temperature 300 K. Single crystals of $[C_3N_2H_5]_5[Bi_2Br_{11}]$ could be also grown from the acetonitrile solution at constant temperature 290 K. Chemical analysis gave the following mass percentages (values in brackets are theoretical): C, 11.01 ± 0.1 (10.97); N, 8.56 ± 0.1 (8.53); H 1.56 ± 0.05 (1.53).

Differential scanning calorimetry (DSC) was recorded using a Perkin Elmer DSC-7 in the temperature range 100–450 K.

The TGA measurements were performed on a Setaram SETSYS 16/18 instrument in the temperature range 300–750 K with a ramp rate 2 K min^{-1}. The scan was performed in flowing nitrogen (flow rate: 1 dm^3 h^{-1}).

The complex electric permittivity $\epsilon^* = \epsilon' - i\epsilon''$ was measured between 100 and 300 K by an Agilent 4284A Precision LCR Meter in the frequency range between 100 Hz and 1 MHz. The dimensions of the sample were approximately $4 \times 4 \times 1$ mm^3. The overall error was less than 5%.

The spontaneous polarization was measured between 100 and 200 K by a charge integration technique using a Keithley 617 Programmable Electrometer. The temperature was stabilized by an Instec STC 200 temperature controller.

X-ray data were collected on a Kuma KM4CCD diffractometer (Mo Kα radiation; $\lambda = 0.710\,73$ Å). X-ray data were collected at 170 and 100 K using an Oxford Cryosystem device. Data reduction and analysis were carried out with the CrysAlice 'RED' program [24]. The space groups were determined using the XPREP program. Structures were solved by Patterson methods using the XS program and refined using all F^2 data, as implemented by the XL program [25]. Non-hydrogen atoms were refined with anisotropic displacement parameters.

Crystallographic data for the structure reported in this paper (excluding structure factors) have been deposited with the Cambridge Crystallographic Data Centre, CCDC numbers: 686163, 686164.

Copies of this information may be obtained free of charge from the Director, CCDC, 12 UNION Road, Cambridge CB2 1EZ, UK (fax: +44 1223 336033; e-mail: deposit@ccdc.cam.ac.uk or http://www.ccdc.cam.ac.uk).

3. Results and discussion

3.1. Thermal properties

Figure 1(a) shows the DSC thermogram for $[C_3N_2H_5]_5[Bi_2Br_{11}]$. The DSC curves were recorded upon heating and cooling at 10 K min^{-1}. The calorimetric measurements show that the crystal under investigation undergoes two fully reversible phase transitions. The higher temperature transition, of first-order type, at ca 355/352 K ± 0.2 is accompanied by a transition entropy (ΔS_{tr}) which was estimated to be about 20.8 ± 3 J mol^{-1} K^{-1}. The lower temperature transition at about 155/155 ± 0.2 with the ΔS_{tr} of the order of 12 ± 2 J mol^{-1} K^{-1} is characterized by a negligible temperature hysteresis. It should be noted that the thermal anomaly seen as a well-shaped peak is characteristic of a first-order transition. Nevertheless, taking into account the fact that we did not see either the temperature hysteresis or the phase front (the observations of the sample by a polarizing microscope close to T_c) the phase transition at 155 K may be classified as a second-order type.

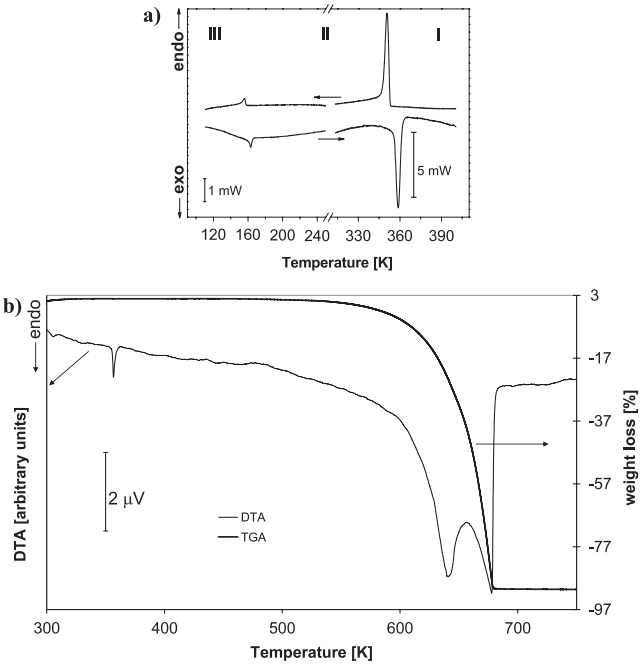

Figure 1. (a) DSC curves for the $[C_3N_2H_5]_5[Bi_2Br_{11}]$ crystal upon cooling and heating runs (10 K min^{-1}, $m = 23$ mg).
(b) Simultaneous thermogravimetric analysis and thermal analysis scan (with temperature rate of 2 K min^{-1}, sample mass 15.7 mg) for $[C_3N_2H_5]_5[Bi_2Br_{11}]$.

Thermal stability of the crystal was studied by means of a simultaneous thermogravimetric analysis (TGA) and differential thermal analysis (DTA) scan between 300 and 750 K. These results, presented in figure 1(b), show that $[C_3N_2H_5]_5[Bi_2Br_{11}]$ exhibits one endothermal peak at about 355 K on the DTA curve, which corresponds to the high temperature transition detected in the DSC measurements. The crystal seems to be stable up to about 500 K and above this temperature a continuous decomposition of the sample takes place.

3.2. Optical observations

The optical observations of the sample under a polarizing microscope at the room temperature phase II showed that the

Table 1. Crystal data and structure refinement for $[C_3N_2H_5]_5[Bi_2Br_{11}]$ at 170 K (phase II) and 100 K (phase III).

Phase	II	III
Empirical formula	$[C_3N_2H_5]_5[Bi_2Br_{11}]$	$[C_3N_2H_5]_5[Bi_2Br_{11}]$
Formula weight (g mol^{-1})	1642.42	1642.42
Temperature	170(2)	100(2)
Wavelength	0.710 73	0.710 73
Crystal system	Monoclinic	Monoclinic
Space group	$P2_1/n$	Pn
a (Å)	9.257(2)	9.099(2)
b (Å)	15.157(3)	15.197(3)
c (Å)	13.865(3)	13.807(3)
β (deg)	97.73(3)	97.94(3)
V (Å^3)	1927.7(7)	1890.9(7)
Z	2	2
Calculated density (g cm^{-3})	2.830	2.885
Absorption coefficient (mm^{-1})	20.541	20.941
F(000)	1472	1472
Crystal size (mm)	0.13 × 0.10 × 0.09	0.13 × 0.10 × 0.09
Theta range for data collection (deg)	3.07–27.00	3.07–27.00
Ranges of h, k, l	$-11 \leqslant h \leqslant 11$	$-11 \leqslant h \leqslant 11$
	$-19 \leqslant k \leqslant 11$	$-19 \leqslant k \leqslant 11$
	$-17 \leqslant l \leqslant 17$	$-17 \leqslant l \leqslant 17$
Reflections collected/unique	12 882/4137	12 612/7902
Refinement method	Full-matrix least-squares on F^2	Full-matrix least-squares on F^2
Data/restraints/parameters	4137/126/241	7902/152/344
Goodness-of-fit on F^2	1.082	1.010
Final R_1/wR_2 indices ($I > 2\sigma I$)	0.0650/0.0702	0.0515/0.0894
R_1/wR_2 indices (all data)	0.1162/0.0792	0.0743/0.0962
Largest diff. peak/hole (eÅ^{-3})	0.863/−0.959	1.220/−1.386

crystal under investigations exhibits a complex ferroelastic domain structure. Unfortunately, during heating, approaching the phase transition II → I from below, the single crystal becomes non-transparent because of some changes on its surface. Thus it is difficult to state if the high temperature phase I is really a paraelastic one. On the other hand all the imidazolium analogs $(C_3N_2H_5)_5Bi_2Br_{11}$, $(C_3N_2H_5)_5Sb_2Br_{11}$ and $(C_3N_2H_5)_5Bi_2Cl_{11}$ appeared to be isomorphic in the room temperature phase and exhibit an identical sequence of phase transitions. X-ray studies on $(C_3N_2H_5)_5Bi_2Cl_{11}$ showed that the high temperature phase transition at 360 K [16] is evidently the ferroelastic–paraelastic type from monoclinic to tetragonal symmetry. Taking into account all the above mentioned facts we suggest that the II → I phase transition at 355 K in $(C_3N_2H_5)_5Bi_2Br_{11}$ is of the ferroelastic–paraelastic type.

3.3. Single crystal x-ray diffraction

Crystallographic data and details on the structures determination of $[C_3N_2H_5]_5[Bi_2Br_{11}]$ at 100 and 170 K are given in table 1. The selected bond lengths and angles are listed in table 2. There is a part of the discrete $[Bi_2Br_{11}]^{5-}$ anion and five nonequivalent imidazolium cations (four types) in an asymmetric part of the unit cell (figure 2). The $[Bi_2Br_{11}]^{5-}$ parts form distorted bioctahedra with one bridging Br1 atom located in a special position (figure 3). Among four crystallographically unrelated imidazolium cations, one, labeled as type A, placed in general positions, is ordered. The other crystallographically unrelated cations (B, C and D types) found close to special positions are disordered and each of the cations is distributed over two positions with the occupancy factors 0.5 (the 180° reorientation model). The imidazolium cations are connected to the $[Bi_2Br_{11}]^{5-}$ parts by weak N–H · · · Br hydrogen bonds (table 3). Comparison of the hydrogen bond system at 170 and 100 K revealed that the most important N–H · · · Br bonds experience a significant shortening. Moreover, additional N–H · · · Br hydrogen bonds appear with decreasing temperature. These changes seem to be the reason for ordering of the imidazolium cations at 100 K.

Figure 4 clearly shows that the anionic substructure does not experience any visible distortion through the phase transition at 155 K. On the other hand important changes are observed within the cationic substructure. Apart from the expected changes in the ordering of the cations of types B, C and D (below 155 K one site is realized) in the case of cation B an important change should be noted in the position of the plane of imidazole ring at two temperatures (100 and 170 K). It means that we have some shift of the nitrogen and carbon atoms through the phase transition. This effect may be treated as a 'displacive' contribution to the phase transition mechanism.

3.4. Temperature measurements of the unit cell parameters

The temperature dependencies of the lattice parameters a, b, c and the β monoclinic angle and volume of the unit cell (V) over the temperature range 100–170 K are shown

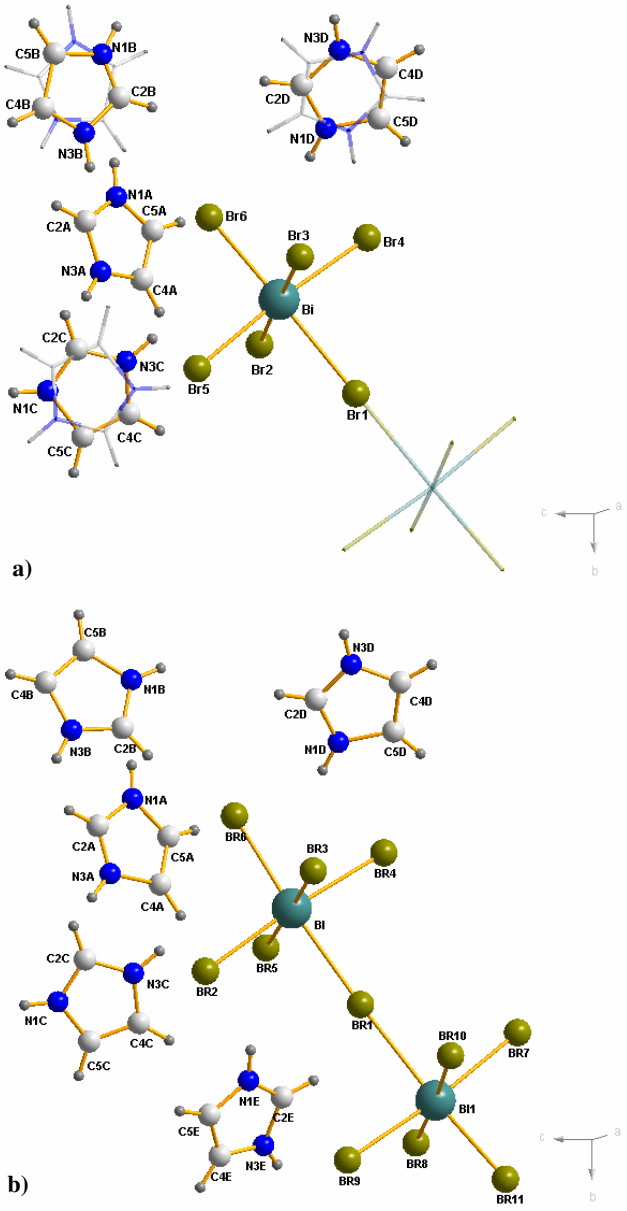

Figure 2. Independent parts of the unit cell of $[C_3N_2H_5]_5[Bi_2Br_{11}]$ at (a) 170 K and (b) 100 K with the atom labeling scheme.

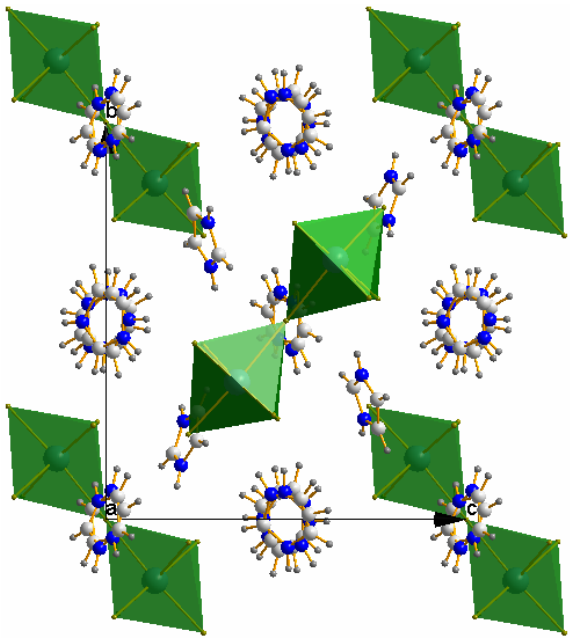

Figure 3. Projection of the crystal structure packing of $[C_3N_2H_5]_5[Bi_2Br_{11}]$, viewed down the a-axis at 170 K, showing the inorganic layer framework along with imidazolium cations.

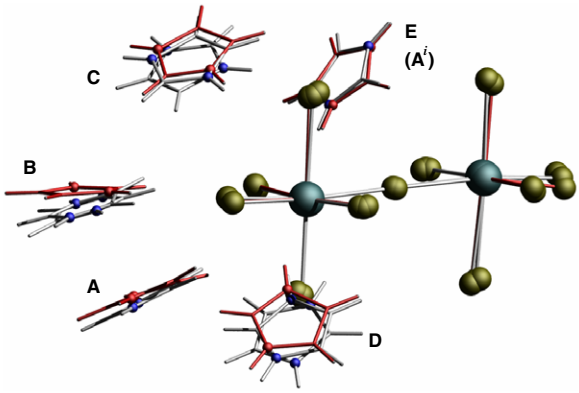

Figure 4. Comparison of the structures in phase II and III (i denotes symmetry code: $0.5 - x, 0.5 + y, 0.5 - z$).

in figures 5(a) and (b), respectively. One subtle structural anomaly of the lattice parameters is observed close to 155 K, which corresponds to the structural phase transition disclosed by DSC measurements. A slight change in the slope appears on the plot of temperature dependence of the a-axis, whereas for the c-axis a diffused peak is visible close to 155 K. The structural anomaly is better shown for the dilation along the b-axis. Above 155 K the b lattice parameter is nearly constant and after crossing the phase transition it increases significantly showing a negative linear thermal expansion coefficient. The plot of lattice volume versus temperature displays a clear structural anomaly (see figure 5(b)). In turn, the monoclinic β-angle keeps its constant value without any visible anomaly near 155 K. Structural dilatometric measurements point out the continuous character of the structural phase transition at 155 K.

3.5. Dielectric measurements

The temperature dependence of the complex electric permittivity, $\epsilon^* = \epsilon' - i\epsilon''$, measured at the frequency 135 Hz along the a, b, and c axes of the monoclinic crystal of $[C_3N_2H_5]_5[Bi_2Br_{11}]$ close to the phase transition II $\rightarrow$ III is presented in figure 6(a). The dielectric permittivity, ϵ', reaches a value of about 420 units at 155 K along the a-axis. Taking into account the fact that ϵ''_a near T_c is rather small (below 0.2) the electric permittivity measured at 135 Hz may be treated as a static one. The ϵ' is half as small along the c-direction, whereas along the b-axis it is nearly one order of magnitude smaller than that measured along the a-axis. According to the results we can state that the monoclinic a-axis is preferred, which is in agreement with a polar monoclinic point group, **m**, (space group Pn) proposed on the basis of x-ray results. In this case the polar direction is expected to appear within the ac plane.

Table 2. Selected bond lengths (Å) and angles (deg) for $[C_3N_2H_5]_5[Bi_2Br_{11}]$ at 170 and 100 K.

170 K		100 K	
Bi–Br6	2.7185(13)	Bi–Br6	2.754(2)
Bi–Br5	2.8415(13)	Bi–Br3	2.785(3)
Bi–Br2	2.9680(14)	Bi–Br2	2.811(2)
Bi–Br3	2.7641(14)	Bi–Br4	2.898(2)
Bi–Br4	2.8750(14)	Bi–Br5	2.923(2)
Bi–Br1	3.0070(6)	Bi–Br1	2.962(3)
		Br1–Bi1	3.036(3)
		Bi1–Br11	2.706(2)
		Bi1–Br8	2.716(2)
		Bi1–Br9	2.851(2)
		Bi1–Br7	2.860(2)
		Bi1–Br10	3.039(2)
Br6–Bi–Br3	90.80(4)	Br6–Bi–Br3	88.65(7)
Br6–Bi–Br5	93.83(5)	Br6–Bi–Br2	96.77(7)
Br3–Bi–Br5	91.76(4)	Br3–Bi–Br2	92.23(8)
Br6–Bi–Br4	90.55(4)	Br6–Bi–Br4	87.21(7)
Br3–Bi–Br4	90.12(4)	Br3–Bi–Br4	92.06(7)
Br5–Bi–Br4	175.21(4)	Br2–Bi–Br4	174.22(7)
Br6–Bi–Br2	89.63(4)	Br6–Bi–Br5	90.64(7)
Br3–Bi–Br2	178.65(4)	Br3–Bi–Br5	178.13(7)
Br5–Bi–Br2	89.48(4)	Br2–Bi–Br5	86.14(6)
Br4–Bi–Br2	88.60(4)	Br4–Bi–Br5	89.64(7)
Br6–Bi–Br1	172.94(3)	Br6–Bi–Br1	172.30(9)
Br3–Bi–Br1	96.08(3)	Br3–Bi–Br1	96.51(9)
Br5–Bi–Br1	87.57(3)	Br2–Bi–Br1	88.76(8)
Br4–Bi–Br1	87.85(3)	Br4–Bi–Br1	86.90(8)
Br2–Bi–Br1	83.46(3)	Br5–Bi–Br1	84.37(8)
Bi[a]–Br1–Bi	180.000(16)	Bi–Br1–Bi1	177.28(11)
		Br11–Bi1–Br8	92.99(7)
		Br11–Bi1–Br9	92.06(7)
		Br8–Bi1–Br9	88.86(7)
		Br11–Bi1–Br7	93.21(7)
		Br8–Bi1–Br7	91.67(8)
		Br9–Bi1–Br7	174.67(7)
		Br11–Bi1–Br1	169.06(8)
		Br8–Bi1–Br1	97.90(9)
		Br9–Bi1–Br1	87.18(8)
		Br7–Bi1–Br1	87.50(8)
		Br11–Bi1–Br10	87.98(7)
		Br8–Bi1–Br10	176.00(7)
		Br9–Bi1–Br10	87.22(7)
		Br7–Bi1–Br10	92.15(6)
		Br1–Bi1–Br10	81.09(8)

[a] $-x+1, -y+2, -z$.

The $1/\epsilon_a$ versus temperature representation (see figure 6(b)) permits us to predict both the order of the phase transition and the Curie–Weiss constants according to the formula:

$$\epsilon'_a = \frac{C_{+/-}}{(T - T_c)} \tag{1}$$

where C_+ and C_- are the constants for the paraelectric and ferroelectric phase, respectively. The linear part of $1/\epsilon_a$ (T) curve is maintained only over a narrow temperature region, of about 2.5 K above and 2 K below 155 K. The ratio $C_+/C_- = 1.75$ is a little smaller than that expected for the second-order ferroelectric transitions ($C_+/C_- = 2$). It should be added, however, that the dielectric permittivity was measured in the dispersion frequency region, thus the C_+ and C_- constants may depend on the frequency of the electric field. Our preliminary low frequency dielectric dispersion studies

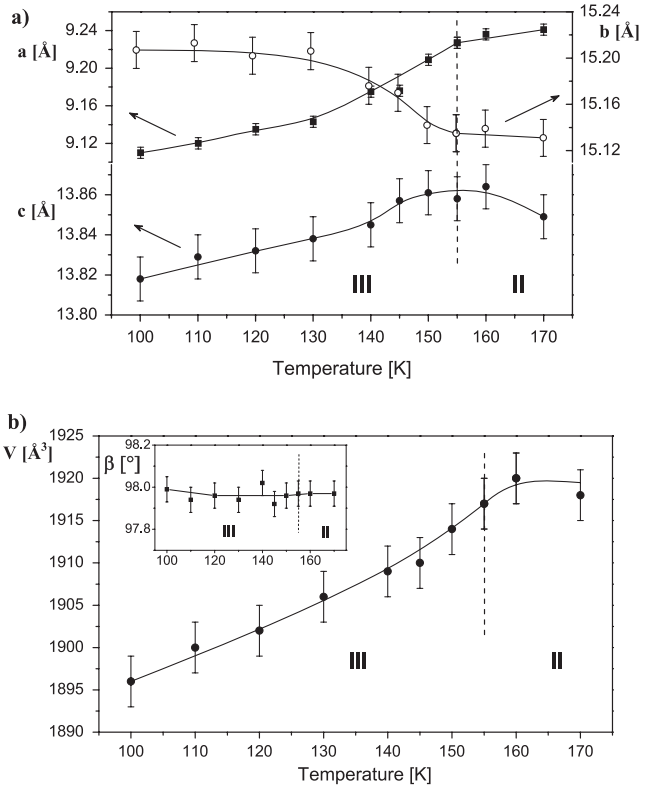

Figure 5. Temperature dependencies of the lattice parameters (a) a, b and c (b) β and V (volume of the unit cell).

Table 3. Hydrogen bonds in $[C_3N_2H_5]_5[Bi_2Br_{11}]$ ((Å) and (deg)) at 170 and 100 K.

D–H···A	d(D–H)	d(H···A)	d(D···A)	<(DHA)
170 K				
N(1A)–H(1A)···Br(5)[a]	0.86	2.54	3.343(9)	155.2
N(3A)–H(3A)···Br(2)[b]	0.86	2.64	3.378(10)	144.9
N(1B)–H(1B)···Br(4)[c]	0.86	2.67	3.51(3)	167.1
N(1C)–H(1C)···Br(2)[d]	0.86	2.56	3.37(3)	157.3
N(3C)–H(3C)···Br(2)	0.86	2.66	3.35(3)	138.3
N(3D)–H(3D)···Br(4)[e]	0.86	2.56	3.39(4)	161.2
100 K				
N(1A)–H(1A)···Br(7)[f]	0.90	2.43	3.290(18)	160.8
N(3A)–H(3A)···Br(5)[g]	0.85	2.63	3.315(19)	138.9
N(1B)–H(1B)···Br(10)[h]	0.89	2.68	3.497(17)	152.8
N(3B)–H(3B)···Br(4)[f]	0.86	2.57	3.400(16)	161.5
N(1C)–H(1C)···Br(10)[i]	0.89	2.51	3.373(15)	162.6
N(3C)–H(3C)···Br(5)	0.76	2.69	3.343(16)	145.0
N(1D)–H(1D)···Br(6)	0.93	2.64	3.483(15)	151.0
N(3D)–H(3D)···Br(9)[j]	0.91	2.47	3.370(17)	171.2
N(1E)–H(1E)···Br(2)	0.83	2.63	3.357(19)	147.5
N(3E)–H(3E)···Br(10)[k]	0.91	2.61	3.409(17)	146.2

[a] $-x+1/2, y-1/2, -z+1/2$; [b] $x-1, y, z$;
[c] $-x+3/2, y-1/2, -z+1/2$; [d] $-x+1, -y+2, -z+1$.
[e] $-x+1, -y+1, -z$; [f] $x-1/2, -y+1, z+1/2$; [g] $x-1, y, z$;
[h] $x+1/2, -y+1, z+1/2$; [i] $x, y, z+1$; [j] $x, y-1, z$;
[k] $x+1/2, -y+2, z+1/2$.

reveal that the relaxation process in $[C_3N_2H_5]_5[Bi_2Br_{11}]$ over the paraelectric phase close to T_c takes place between 10^2 and 10^4 Hz. The results obtained can be explained by the critical

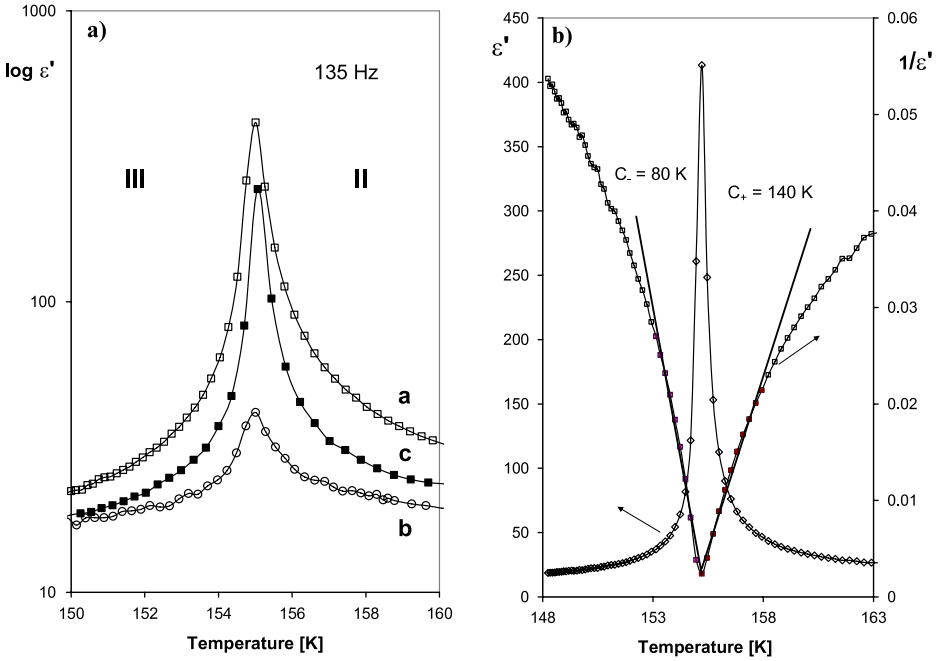

Figure 6. (a) Complex electric permittivity, $\epsilon^* = \epsilon' - i\epsilon''$, measured at the frequency 135 Hz along the a, b and c axes of the monoclinic system for $[C_3N_2H_5]_5[Bi_2Br_{11}]$ in the vicinity of the ferroelectric phase transition (II → III), (b) $1/\epsilon'_a$ versus temperature representation. (The Curie–Weiss law.)

slowing-down of the polarization relaxation process. The full analysis of the dielectric response function will be presented elsewhere [26].

3.6. Pyroelectric measurements

The crystal under investigations is characterized by a quite slow switching process and relatively high coercive field (higher than 10 kV cm^{-1}) and this is a reason that no ferroelectric hysteresis loop was observed using a Diamond-Dreck-Pepinsky bridge with an electric field of the 50–10 Hz frequency. It should be added, that in the case of other imidazolium ferroelectrics like: $[C_3N_2H_5]_5[Bi_2Cl_{11}]$ and $[C_3N_2H_5]_5[Sb_2Br_{11}]$, the ferroelectric hysteresis loops could be observed at an extremely slow frequency of the order of 0.01 Hz. To confirm the ferroelectric properties in $[C_3N_2H_5]_5[Bi_2Br_{11}]$ pyroelectric measurements were undertaken. The pyroelectric current was measured after poling the crystal while cooling from 200 K down to about 100 K. The dc electric field was equal to +8 kV cm^{-1}. Then the pyroelectric current, (I_{pyro}) was measured during the heating cycle. The same procedure was applied after poling the crystal by a dc electric field of negative value −8 kV cm^{-1}. The calculated spontaneous polarization P_s as a function of temperature is shown in figure 7. The spontaneous polarization (P_s) is reversed by the external dc electric field. This is a crucial proof of the evidence of ferroelectric properties below 155 K. The P_s value is found to be about 2.6×10^{-3} C m^{-2} at 130 K (figure 7). The inset shows ln P_s as a function of $\ln(T_c - T)^{\beta}$, where β denotes the critical exponent, which for ferroelectric compounds ranges from 0.50 to 1 for the continuous phase transition. For the

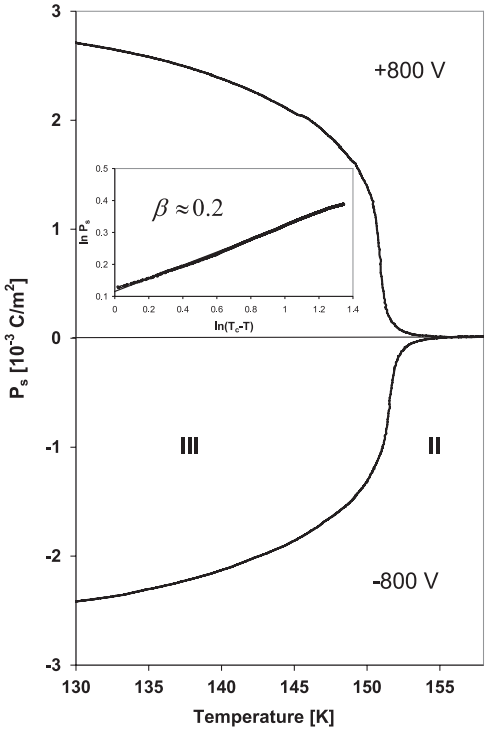

Figure 7. Spontaneous polarization (P_s) as a function of temperature from the pyroelectric effect for the poling electric field ±8 kV cm^{-1}. The inset shows ln P_s as a function of $\ln(T_c - T)$.

crystal under investigation a linear dependence of this function, over the temperature range 4 K is observed with a parameter equal to about 0.20. It should be added, that the β-value is significantly smaller than that expected from theory for the continuous transition.

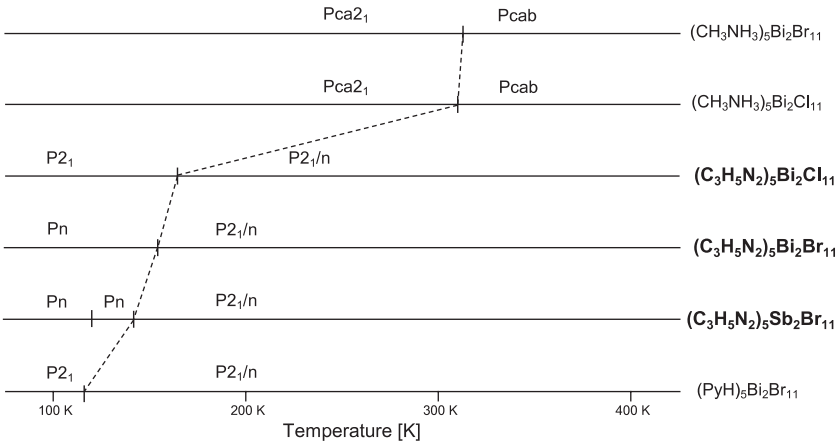

Figure 8. Phase situation in $R_5M_2X_{11}$-type ferroelectrics.

4. Discussion

So far, we have synthesized and characterized six compounds crystallizing with the $R_5M_2X_{11}$ chemical composition. All of them, in general, are characterized by substantial structural similarities. The crystal structures consist of discrete $[M_2X_{11}]^{5-}$ bioctahedral units and five crystallographically unrelated organic cations, which exhibit various dynamic disorder in the paraelectric phase.

The size of the organic cations imbedded in the anionic substructure modifies the phase transition sequence—both the temperature of the paraelectric–ferroelectric transition and the space group symmetry of subsequent phases. The analogs containing small size methylammonium cations, undergo the paraelectric–ferroelectric transition within the orthorhombic symmetry: $Pcab \rightarrow Pca2_1$, at 311 $[CH_3NH_3]_5[Bi_2Br_{11}]$ and at 307 K $[CH_3NH_3]_5[Bi_2Cl_{11}]$. The comparison of the phase situation in all studied $R_5M_2X_{11}$-type ferroelectrics is illustrated in figure 8.

The replacement of the methylammonium cations into larger aromatic cations like imidazolium or pyridinium, significantly shifts the Curie point towards lower temperature by about 150–200 K. In addition, the symmetry of both the paraelectric and ferroelectric phase decreases from orthorhombic (methylammonium cations) to monoclinic symmetry (aromatic parts). Despite these obvious structural differences, the common feature of all $R_5M_2X_{11}$-type compounds are the following experimental facts concerning the paraelectric–ferroelectric transitions at ambient pressure:

- The nature of ferroelectric transitions is continuous.
- The transitions are classified as an 'order–disorder' type.
- The molecular mechanism of the paraelectric–ferroelectric transition is found to be due to a motion of the organic cations. In the paraelectric phase two of five crystallographically unrelated cations placed in the general positions are ordered and do not contribute to the ferroelectric properties. The remaining three crystallographically unrelated cations (placed in the special positions) are disordered being distributed over two sites. In the ferroelectric phase they became ordered, continuously with temperature, being fully ordered at temperatures at which one can observe saturated spontaneous polarization.

It is worth emphasizing that despite the analogous mechanism of phase transition for 'methylammonium' and 'aromatic' analogs the strength of dipole–dipole interactions of ferroelectric type is quite different, which is directly reflected in the magnitudes of the spontaneous polarization (P_s) and electric permittivity (ϵ). P_s is 2–3 $\times$ 10^{-2} and 2–6 $\times$ 10^{-3} C m^{-2}, whereas ϵ_{max} is 1–2 $\times$ 10^4 and 2–6 $\times$ 10^2 for the methylammonium and aromatic analogs, respectively.

It means that interactions, which lead to a long-range ferroelectric order are significantly stronger in the case of the methylammonium analogs. Hence, the ferroelectric phase of the methylammonium analogs is exists preferentially at higher temperatures. The next feature which differentiates both subgroups of the discussed compounds is the dynamic dielectric properties. The dielectric relaxators for methylammonium analogs appear in the microwave frequency region (10^{-8}–10^{-10} Hz) whereas the 'aromatic' compounds are characterized by an extremely low frequency region of the relaxation process (10^{-2}–10^{-4} Hz). The mobility of the cations is not directly connected with the strength of the dipole–dipole interaction, because these two effects give an opposite contribution for the above discussed crystal. Most intriguing in the $R_5M_2X_{11}$-type ferroelectric is the mechanism of ferro-paraelectric phase transition. Two contributions should be considered: (i) order–disorder and (ii) displacive. The contribution of (i) is assigned to a motion of the organic cations. It is well reflected in the dielectric dispersion and the entropy effects. The cations are also expected to contribute to the spontaneous polarization. The contribution of (ii) is not directly confirmed by any experimental technique. However, it may be assigned to the deformation of the anionic substructure (or bioctahedral units) seen in the x-ray studies.

The last feature is the most characteristic feature which distinguishes methylammonium from aromatic analogs. In the case of the former compounds, during the phase transition of the $[CH_3NH_3]_5[Bi_2Cl_{11}]$ octahedral subunits of the anionic bioctahedron experience twisting around the Bi–Bi axis from

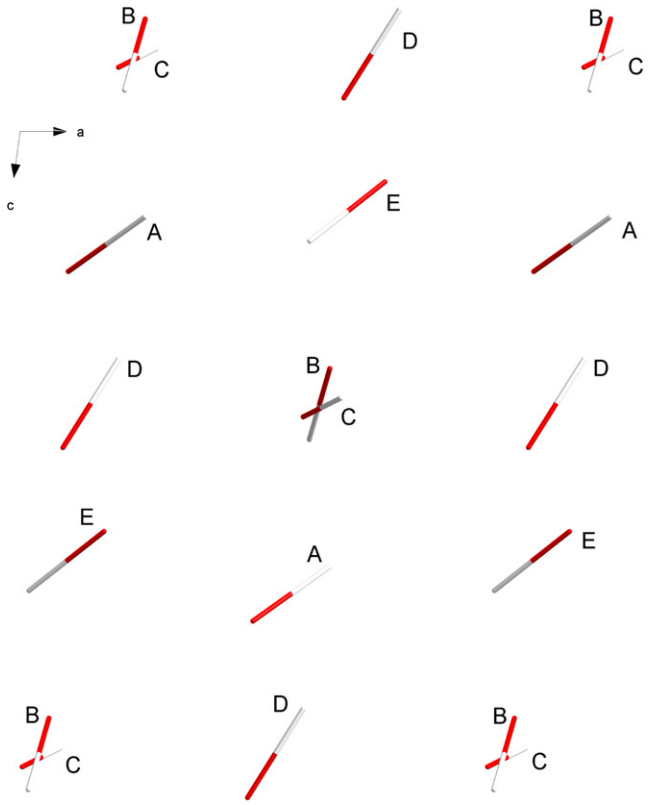

Figure 9. Mutual orientation of the dipole moments in the unit cell along the [010] direction at 100 K (vector's representation). Vector is defined by the C atom placed between two N atoms and the center of the C–C bond of the cation.

about 0° up to 16°. On the other hand, during phase transition of aromatic analogs the reciprocal arrangement of octahedral subunits remains practically unchanged. It means that in contrast to that found for the methylammonium complexes, 'aromatic' analogs do not experience a visible distortion of the anionic substructure. In our opinion it may be connected with the 'lone' pair effect ($5s^2$ for Sb(III) or $6s^2$ for Bi(III)) which is more enhanced for the methylammonium analogs discussed above. The role of lone pair of the antimony (III) and bismuth (III) atoms is still unsolved. Nevertheless, one can expect an important contribution of the lone pair to the electric polarization of the system. Comparison of the crystal structure of $[C_3N_2H_5]_5[Bi_2Br_{11}]$ at two temperatures (170 and 100 K) leads to interesting remarks. The dipole moment of the imidazolium cation is directed along the line passing through the carbon atom bonded to the nitrogen atoms and the center of the C–C bond. At 170 K the crystal structure was refined in $P2_1/n$, thus suitable cations are related by the center of symmetry, and the resultant dipole moment of the unit cell is practically negligible in the paraelectric phase. The situation changes substantially over the ferroelectric phase. The orientation of dipoles of the cations in the unit cell viewed along the b-axis at 100 K is shown in figure 9. In phase III, below 155 K, the relative orientation of the cations type A and E in relation to the anionic bioctahedron is almost the same as the orientation of the A and A $(0.5 - x, 0.5 + y, 0.5 - z)$ cations in the phase II at 170 K (figure 9). Thus, the A and E cations do not contribute to P_s. The cations type B, C and D, which in the centrosymmetric space group at 170 K reveal disorder, are ordered in the noncentrosymmetric space group at 100 K. Thus, they should contribute to the resultant dipole moment of the cationic substructure. In an endeavor to determine the relative magnitude of the moment dipole in the [100], [010] and [001] directions, we calculated the resultant vector of the moment dipole. Vectors of the moment dipole of particular cations B, C and D were defined by the start at the center of the C–C bond and the end at the C atom situated between two nitrogen atoms. Taking into account the symmetry operator, [−2.66 0.02 1.42] represents the resultant vector of the unit cell. The resultant vector demonstrates that the cations contribute mainly to the spontaneous polarization within the ac plane, and the effect is about twice as strong in the [100] direction as in the [001] direction. The effect is negligible in the [010] direction. The value of P_s for all known aromatic ferroelectrics of $R_5M_2X_{11}$-type is relatively small being of the order of 2–6 $\times$ 10^{-3} C m^{-2}. We should also remember that some part of the resultant dipole moment of the unit cell is expected to originate from the hydrogen bond configuration (N–H $\cdots$ Br) of the system. Thus, the final resultant dipole moment within the ac plane may deviate from that which originates from the entire dipole of cations.

5. Conclusion

(1) $[C_3N_2H_5]_5[Bi_2Br_{11}]$ was found to undergo two solid–solid phase transitions:
I $\xrightarrow{355\,K}$ II first-order type;
($P2_1/n$) II $\xrightarrow{155\,K}$ III (Pn) second-order type.

(2) The crystal structure of $[C_3N_2H_5]_2[Bi_2Br_{11}]$ consists of a discrete corner-sharing bioctahedra $[Bi_2Br_{11}]^{5-}$ and five crystallographically unrelated imidazolium cations (type A, B, C and D). In the phase II the cations A are ordered, whereas B, C and D are highly disordered and distributed over two sites (occupancy 0.50/0.50). In the low temperature phase III all the cations are fully ordered.

(3) $[C_3N_2H_5]_5[Bi_2Br_{11}]$ was found to be a ferroelectric compound with the Curie temperature 155 K and a saturated spontaneous polarization of about 2.6 $\times$ 10^{-3} C m^{-2}, which is characteristic of 'weak' ferroelectric materials.

(4) The ferroelectric phase transition (II $\rightarrow$ III) mechanism is due to the dynamics of dipolar imidazolium cations (type B, C and D), which contribute predominantly to the spontaneous polarization and determine the critical behavior of the dielectric permittivity of $[C_3N_2H_5]_2[Bi_2Br_{11}]$. The single crystal x-ray and calorimetric studies suggest an 'order–disorder' mechanism for the ferroelectric phase transition.

Acknowledgment

This work was supported by the Polish State Committee for Scientific Research (Project Register No. N204 108 31/2551).

References

[1] Mitzi D B 1999 *Prog. Inorg. Chem.* **48** 1
[2] Papavassiliou G C 1997 *Prog. Solid State Chem.* **25** 125
[3] Era M 2003 *Chem. Lett.* **32** 272
[4] Coe S, Woo W K, Bawendi M and Bulovic V 2002 *Nature* **420** 803
[5] Jakubas R and Sobczyk L 1990 *Phase Transit.* **20** 163
[6] Jakubas R, Sobczyk L and Zaleski J 1997 *Pol. J. Chem.* **71** 265
[7] Bujak M and Zaleski J 2004 *J. Solid State Chem.* **177** 3202
[8] Ishihara H, Watanabe K, Iwata A, Yanida K, Kinoshita Y, Okuda T, Krishnan V G, Dou S and Weiss A 1992 *Z. Naturf.* **47** 65
[9] Ishihara H, Yamada K, Okuda T and Weiss A 1993 *Bull. Chem. Soc. Japan* **66** 380
[10] Iwata M, Eguchi M, Ishibashi Y, Sasaki S, Shimizu H, Kawai T and Shimanuki S 1993 *J. Phys. Soc. Japan* **62** 3315
[11] Zaleski J and Pietraszko A 1996 *Acta Crystallogr.* B **52** 287
[12] Zaleski J, Pawlaczyk Cz, Jakubas R and Unruh H G 2000 *J. Phys.: Condens. Matter* **12** 7509
[13] Carpentier P, Lefebvre J and Jakubas R 1995 *Acta Crystallogr.* B **51** 167
[14] Mróz J and Jakubas R 1989 *Solid State Commun.* **72** 813
[15] Jóźków J, Bator G, Jakubas R and Pietraszko A 2001 *J. Chem. Phys.* **114** 7239
[16] Jakubas R, Piecha A, Pietraszko A and Bator G 2005 *Phys. Rev.* B **72** 104107
[17] Piecha A, Pietraszko A, Bator G and Jakubas R 2008 *J. Solid State Chem.* **181** 1155
[18] Carpentier P, Zielinski P, Lefebvre J and Jakubas R 1997 *J. Phys.: Condens. Matter* **102** 403
[19] Piecha A, Bator G and Jakubas R 2005 *J. Phys.: Condens. Matter* **17** L411
[20] Piecha A and Jakubas R 2007 *J. Phys.: Condens. Matter* **19** 621
[21] Jakubas R, Sobczyk L and Lefebvre J 1989 *Ferroelectrics* **100** 143
[22] Pawlaczyk Cz, Motsch H, Jakubas R and Unruh H-G 1990 *Ferroelectrics* **180** 127
[23] Fatuzzo E and Merz W J 1967 *Ferroelectricity* (Amsterdam: North-Holland)
[24] *CrysAlis RED, ver. 1.171* 1995–2003 Oxford Diffraction, Poland
[25] 1999 *SHELXTL-NT (version 5.1)* Bruker AXS Inc., Madison, WI
[26] Piecha A and Jakubas R 2008 *J. Phys.: Condens. Matter* submitted